nature chemistry

ARTICLES

PUBLISHED ONLINE: 29 JULY 2012 | DOI: 10.1038/NCHEM.1408

# A switching cascade of hydrazone-based rotary switches through coordination-coupled proton relays

Debdas Ray, Justin T. Foy, Russell P. Hughes and Ivan Aprahamian*

**Imidazole, a subunit of histidine, plays a crucial role in proton-relay processes that are important for various biological activities, such as metal efflux, viral replication and photosynthesis. We show here how an imidazolyl ring incorporated into a rotary switch based on a hydrazone enables a switching cascade that involves proton relay between two different switches. The switching process starts with a single input, zinc(II), that initiates an *E*/*Z* isomerization in the hydrazone system through a coordination-coupled proton transfer. The resulting imidazolium ring is unusually acidic and, through proton relay, activates the *E*/*Z* isomerization of a non-coordinating pyridine-containing hydrazone switch. We hypothesize that the reduction in the acid dissociation constant of the imidazolium ring results from a combination of electrostatic and conformational effects, the study of which might help elucidate the proton-coupled electron-transfer mechanism in photosynthetic bacteria.**

Proton relay is ubiquitous in biological systems[1] because it plays a crucial part in many processes, including viral replication[2–4], photosynthesis[5–8], metal efflux[9–11] and enzymatic catalysis[12,13]. The proton translocation in these systems is directed mainly by an intricate network of water channels and/or flexible protonatable protein side chains[14]. Although it is very challenging to mimic such complex proton-conduction pathways[15], one can still be inspired by these systems and build prototypes that can attempt to replicate their function[16]. A common motif in most of the biological proton-relay processes is the imidazolyl ring[2–16], which is a subunit of the amino acid histidine. For example, proton conduction in influenza M2 proton channels is regulated by a dynamically assisted proton-shuttling process[8] (that is, deprotonation of imidazolium units assisted by ring flipping)[4], which is a crucial step in the virus's replication cycle. Alternatively, a coordination-coupled deprotonation (CCD) process that involves histidine residues provides the energetic basis for zinc(II) efflux in a cation-diffusion facilitator[4–9]. However, the coordination of zinc(II) within bacterial photosynthetic reaction centres (RCs) lowers the acid dissociation constant ($pK_a$) of the surrounding histidine residues, which leads to the disruption of proton-transfer pathways and subsequently diminishes electron-transfer rates in the RCs[6–8].

Biological processes play an integral role in the field of molecular switches and machines[17–20] because they are a constant source of inspiration. For some time now we have looked actively into mimicking biological processes[22] in the activation of hydrazone-based[22–25] molecular switches. Our efforts in this direction led to the development of a molecular switch that undergoes configurational switching (that is, *E*/*Z* isomerization), which is activated by zinc(II)-initiated CCD[25]. In the first generation of these switches, a pyridyl ring was used as the proton acceptor. We reasoned that replacing the pyridyl ring with an imidazolyl ring will enable us to investigate the diverse mechanisms and pathways by which this group is involved in biological proton relay (for example, dynamic proton shuttling, CCD, $pK_a$ modulations).

Here we report the synthesis and acid- and zinc(II)-initiated *E*/*Z* isomerization of an imidazole-containing hydrazone switch (**QIH-Me**). More importantly, we show that once the imidazolium ring is formed by the zinc(II)-initiated CCD process, it can itself act as a proton source that can activate a different non-coordinating pyridine-containing hydrazone switch (**PPH**)[24] through a dynamically assisted proton relay (Fig. 1). The key factor behind this switching cascade is a synergistic effect that involves the imidazolyl ring and zinc(II) and leads to a substantial reduction in the $pK_a$ of the imidazolium ring through allosteric and electrostatic regulation. To the best of our knowledge this is the first example of such a multistep switching cascade, and a first instance of a dynamically switched compound that acts as the input to another. This is somewhat reminiscent of the biological molecular motor adenosine triphosphate synthase[26], which through its mechanical operation produces the fuel to power other biological machines.

## Results

The synthesis of **QIH-Me** is achieved in four steps (Fig. 2). First, 1-benzyl-2-methyl imidazole is treated with ethyl chloroformate to obtain **2** (ref. 27). Debenzylation of **2** (10% Pd/C) in ethanol followed by coupling with the quinoline-8-diazonium tetrafluoroborate salt and purification by column chromatography (hexanes: ethyl acetate, 9:1) gives **QIH** in 25% isolated yield. Treatment of **QIH** with methyl iodide in the presence of $K_2CO_3$ gives **QIH-Me** as a yellow solid in 48% yield. **QIH-Me** was characterized by $^1$H and $^{13}$C NMR spectroscopies, high-resolution mass spectrometry and X-ray crystallography (see Supplementary Information).

The fully characterized $^1$H NMR spectrum of **QIH-Me** in $CD_3CN$ (see Supplementary Fig. S4a) shows the presence of a distinct intramolecular hydrogen bond between the hydrazone proton and the imidazolyl and quinolinyl nitrogens. This hydrogen bond manifests itself by a deshielded NH proton signal at $\delta =$ 13.4 ppm. Nuclear Overhauser enhancement spectroscopy (NOESY) experiments clearly show an interaction between proton H8 from the imidazole ring and the hydrazone NH proton, and thus establish that the *E* isomer is the major configuration (>99%) in solution.

Crystals of **QIH-Me** suitable for X-ray analysis were obtained from a 1:1 mixture of $CH_2Cl_2$ and hexanes. The crystal structure

Department of Chemistry, Dartmouth College, 6128 Burke Laboratory, Hanover, New Hampshire 03755, USA. *e-mail: ivan.aprahamian@dartmouth.edu

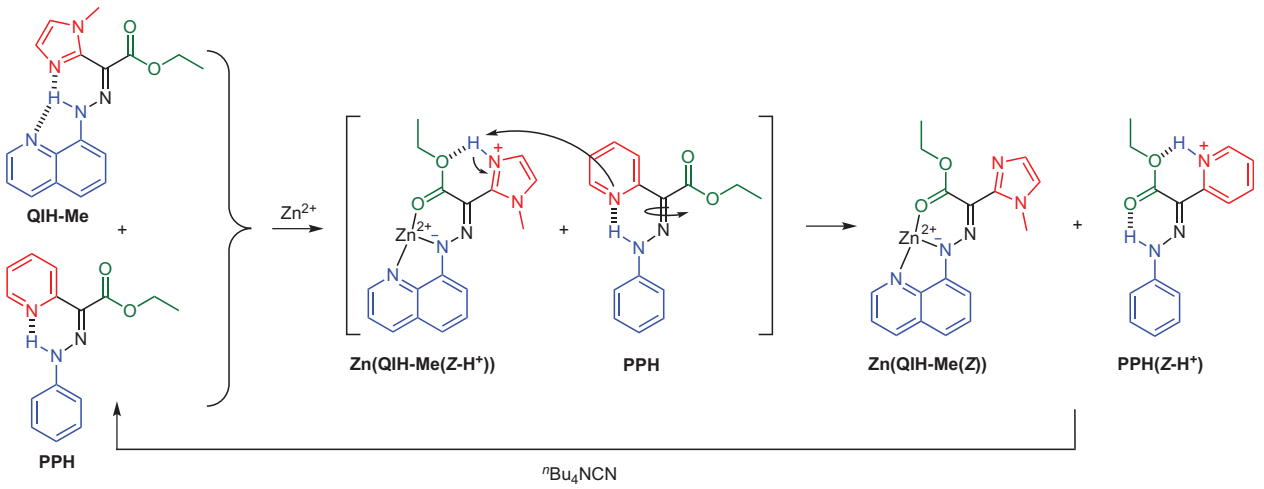


**Figure 1 | Modulating two switches using a single input.** The addition of zinc(II) to a solution of **QIH-Me** and **PPH** initiates a CCD process that switches **QIH-Me** into a system with an unusually acidic imidazolium ring (**Zn(QIH-Me(*Z*-H$^+$))**). The latter, in turn, acts as a trigger that activates **PPH** through proton relay. This whole process is reversible, as the systems revert to their original state on the addition of $^n$Bu$_4$NCN to the reaction mixture.

(Fig. 3a) shows an intramolecular hydrogen bond (N–H···N, 2.731(1) Å, 129.7(0)°) between the imidazolyl nitrogen (N5) and the hydrazone NH proton. The quinolinyl nitrogen atom N3 also forms an intramolecular hydrogen bond (N–H···N, 2.670(1) Å, 103.7(4)°) with the hydrazone proton. The measured dihedral angles indicate that the naphthyl and imidazolyl rings deviate from planarity (–178.11(1)° and 31.47(18)° when viewed along the C(1)–N(1)–N(2)–C(9) atoms and the N(5)–C(5)–C(1)=N(1) atoms, respectively). Comparison of the bond lengths with those of similar intramolecularly hydrogen-bonded hydrazones[28] leads us to conclude that the quinolinyl ring is in conjugation with the imidazolyl and/or ester moieties.

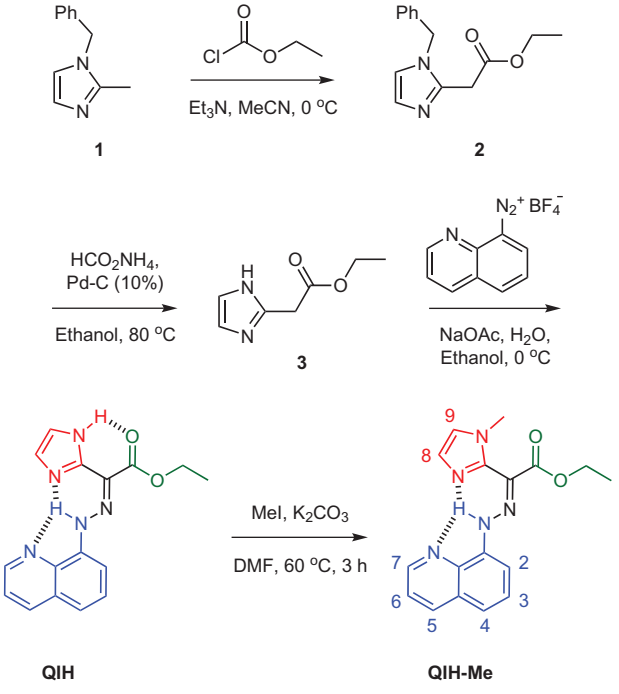


**Figure 2 | Synthesis of QIH-Me.** The alkylation of 1-benzyl-2-methylimidazole (**1**) with ethyl chloroformate to afford **2** (29%) was followed by debenzylation (10% Pd/C) in ethanol to give **3** in 95% yield. Compound **3** was then deprotonated with sodium acetate and coupled with the appropriate diazonium salt to give **QIH-Me** in 25% yield. The latter was treated with methyl iodide in the presence of $K_2CO_3$ to give **QIH-Me** in 48% yield. The methylated derivative used in the studies to simplify the NMR spectra. DMF = dimethyl formamide.

The ultraviolet/visible spectrum of **QIH-Me** ($10^{-5}$ M, $CH_3CN$) shows an absorption maximum ($\lambda_{max}$) at 385 nm (Fig. 4). On titration with zinc(II) perchlorate ($Zn(ClO_4)_2$), the $\lambda_{max}$ shifts bathochromically with an accompanying hypsochromic change. No difference in absorption was observed on the addition of more than 1.0 equiv. of the metal ions. An isosbestic point is observed at $\lambda = 405$ nm, which indicates the interconversion of only two species in solution. A Job's plot analysis (see Supplementary Fig. S32) shows a vertex around 0.55, which suggests a 1:1 binding stoichiometry between **QIH-Me** and $Zn^{2+}$. The binding constant between **QIH-Me** and $Zn^{2+}$ was determined to be $K_1 = 2.7 \times 10^5$ M$^{-1}$. At a higher concentration of **QIH-Me** ($10^{-4}$ M, $CH_3CN$) clear isosbestic points were not observed and the Job's plot analysis shows a vertex at 0.70. This indicates that other species are present in the solution at higher concentrations (see Supplementary Figs S33 and S34).

The binding of $Zn^{2+}$ with **QIH-Me** was also probed using $^1$H NMR spectroscopy. On the addition of $Zn(ClO_4)_2$ to **QIH-Me** the $^1$H NMR spectrum changed drastically: initially, a complicated spectrum was obtained (see Supplementary Fig. S9), which simplified when 8.0 equiv. of $Zn^{2+}$ were added (Fig. 5e). Based on our analysis of the data (1D and 2D NMR spectroscopy) the coordination of $Zn^{2+}$ with **QIH-Me** leads to a coordination-coupled proton transfer that initiates an *E*/*Z* isomerization to give the zinc-bound and protonated complex **Zn(QIH-Me(*Z*-H$^+$))** (ref. 22). This conclusion is based on (i) a NOESY correlation between H2 and the NMe hydrogen atoms, which indicates that an *E* to *Z* isomerization occurred on binding with $Zn^{2+}$ (see Supplementary Fig. S14), and (ii) a correlation spectroscopy (COSY) interaction between the proton at $\delta =$ 11.6 ppm (Im-NH$^+$) and proton H8 on the imidazolyl ring, which indicates that the ring was protonated. This assignment is confirmed by the dissolution of the crystals (see Supplementary Fig. S11) that were used in the analysis of the solid-state structure of the 1:1 complex between $Zn^{2+}$ and **QIH-Me** (Fig. 3b). The $^1$H NMR spectrum obtained from these crystals contains the same signals as those when excess $Zn^{2+}$ was added to **QIH-Me** (Fig. 5e). The spectrum of the crystals also contains signals that arise from a small amount of protonated **QIH-Me** (**QIH-Me(*Z*-H$^+$)** (Fig. 5f)), which indicates that the two species are in equilibrium. The coordination-coupled isomerization process is fully reversible, as illustrated by the $^1$H NMR spectrum obtained after the addition of excess $^n$Bu$_4$NCN to the 1:1 complex (see Supplementary Fig. S23).

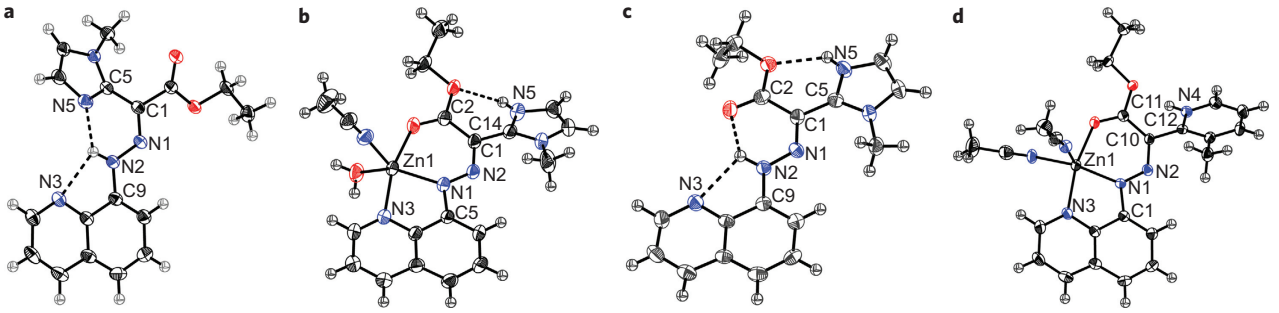


**Figure 3 | Oak Ridge thermal ellipsoid plots (50% probability ellipsoids) of the X-ray crystal structures of the hydrazone-based switches. a–d, QIH-Me (a), zinc(II)-bound and protonated QIH-Me (b), protonated QIH-Me (c) and zinc(II)-bound and protonated QPH-Me (d).** The protons are placed in calculated positions, except for those on the hydrazone N(2), imidazolyl N(5) and pyridyl N(4) atoms, in addition to the water molecule in (**b**), which were refined. The zinc atom in (**b**) is also coordinated with water and acetonitrile molecules, whereas in (**d**) it is coordinated with two acetonitriles. The counterions are removed for the sake of clarity.

At lower concentrations of $Zn^{2+}$ (for example, 0.5 equiv.) three different species were present in solution: **QIH-Me(*Z*-H$^+$)**, **Zn(QIH-Me(*Z*-H$^+$))** and **Zn(QIH-Me(*Z*))** (see Supplementary Figs S9 and S10). This assignment is based on comparison with the spectra of the protonated **QIH-Me** system (Fig. 5f) and the zinc(II)-bound **QIH-Me** complex (Fig. 5g and Supplementary Fig. S18). It seems that at lower concentrations of $Zn^{2+}$ a fraction of the latter acts as an acid to protonate the unbound **QIH-Me** in solution. This process is an indication that the imidazolium nitrogen in **Zn(QIH-Me(*Z*-H$^+$))** is less basic than that in **QIH-Me** (and in pyridine, *vide infra*). The three species are all in equilibrium as the addition of excess $Zn^{2+}$ pushes the equilibrium towards the zinc(II)-bound and protonated **QIH-Me** complex (Fig. 5e).

The self-protonation of **QIH-Me** in the presence of $Zn^{2+}$ is very promising as far as proton relay is concerned. To take advantage of this process, a second non-coordinating rotary switch, **PPH** (ref. 24), was used to probe the possibility of proton relay from **Zn(QIH-Me(*Z*-H$^+$))**. Based on our experimental results we conclude that a coordination-coupled proton transfer initially switches **QIH-Me** into **Zn(QIH-Me(*Z*-H$^+$))** (Fig. 1), which in turn relays its acidic imidazolium proton to **PPH** and transforms it into **PPH(*Z*-H$^+$)**. This whole process is reversible; the addition of $^n$Bu$_4$NCN to the mixture reverts the two switches back to their original state (see Supplementary Fig. S24). Our conclusion with regard to the proton-relay process is based on the following NMR spectroscopy experiments. The $^1$H NMR spectrum of the equimolar mixture of **QIH-Me** and **PPH** (Fig. 5b) shows sharp and non-overlapping signals for the hydrazone and aromatic protons, except for protons H10, H11 and H14, which are merged together at $\delta = 7.38$ ppm. The $^1$H NMR spectrum of the mixture changes drastically, especially for the hydrazone and aromatic hydrogen atoms, when 1.0 equiv. of $Zn^{2+}$ is added to the mixture (Fig. 5c); the aromatic signals of the two switches are well separated, except for protons H5, H16, H2, H3 and H6, and a new signal appears at $\delta = 12.9$ ppm. The general trend is of a downfield shift of the aromatic signals, except for the hydrogen atom H13, which is shifted to a higher field. Based on our earlier report[24] the signal at $\delta = 12.9$ ppm is an indication that the pyridyl ring in **PPH** is protonated at this stage. A comparison with the separately protonated species (Fig. 5d) shows that this is, indeed, the case.

To identify the other species in the solution mixture we conducted a number of control experiments. The addition of 1.0 equivalents of trifluoroacetic acid to **QIH-Me** (Fig. 5f and Supplementary Fig. S22) resulted in a downfield shift of the aromatic signals, and the imidazolyl hydrogen atoms H8 and H9 appear together at $\delta = 7.45$ ppm. In addition, two new signals are observed at $\delta = 14.1$ and 11.9 ppm. The hydrazone NH signal ($\delta = 14.1$ ppm) shows the typical NOESY correlation with proton H7. The broadness of the signal at $\delta = 11.9$ ppm precluded the observation of any COSY or NOESY correlations. We assume that this signal originates from the imidazolium ring (Im-NH$^+$), which would explain the downfield shift of the imidazolyl hydrogen atoms H8 and H9. Moreover, a NOESY interaction between the H2 and Im-Me protons indicates that an *E*/*Z* isomerization has taken place at this stage, as shown by the X-ray analysis of **QIH-Me(*Z*-H$^+$)** (Fig. 3c). The absence of the low-field signals at $\delta = 14.1$ and 11.9 ppm in Fig. 5c is an indication that this species is not present in the two-switch solution mixture. We come to the same conclusion when we compare the mixture with the spectrum of **Zn(QIH-Me(*Z*-H$^+$))** (Fig. 5e). However, the imidazole signals at $\delta = 7.4$ (H8) and 7.2 (H9) ppm, and the aromatic proton signals at $\delta = 8.9$ (H7), 8.5 (H5), 7.7–7.8 (H2/6), 7.6 (H4) and 7.5 (H3) ppm in Fig. 5b, closely match those of **Zn(QIH-Me(*Z*))** (Fig. 5g), which indicates that this species is the second compound in solution.

The most crucial part of the relay process is the lowering of the p$K_a$ of the imidazolium ring by ~3 units[8] in **Zn(QIH-Me(*Z*-H$^+$))**, because without it the multistep switching cascade could not occur. In biological systems, such p$K_a$ modulations are prevalent[1] and usually they are attributed to conformational changes as a result of metal binding. Another relevant mechanism[8,29,30], albeit

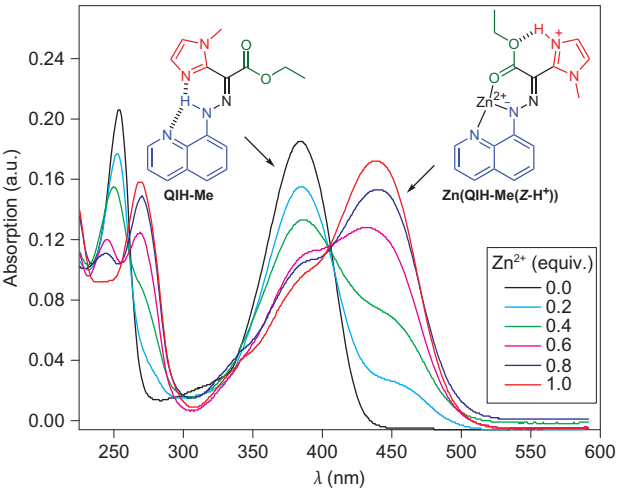


**Figure 4 | Spectroscopic studies of the binding between zinc(II) and QIH-Me ($1.0 \times 10^{-5}$ M, $CH_3CN$, 294 K).** The ultraviolet/visible spectra show a gradual bathochromic shift on titration of **QIH-Me** with $Zn(ClO_4)_2$: $\lambda_{max}$ shifts from 385 nm (black trace) to 438 nm (red trace). An isosbestic point is visible at $\lambda = 405$ nm. The process reaches saturation after the addition of 1.0 equiv. of zinc(II) to **QIH-Me**.

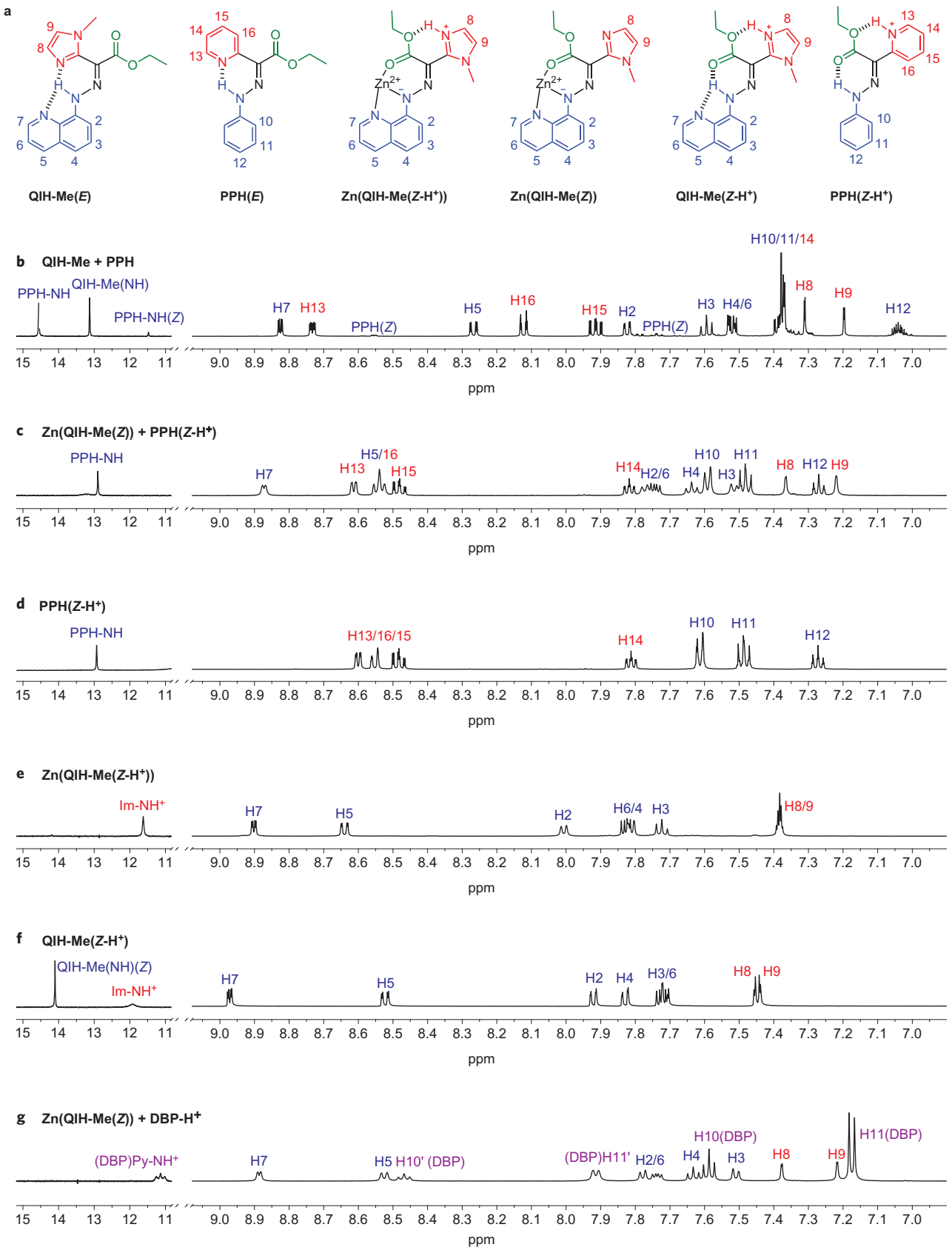


**Figure 5 | The $^1$H NMR spectra (500 MHz, $CD_3CN$, 294 K) used in confirming the CCD-initiated proton transfer that leads to the successive activation of two switches. a**, The structures of the different hydrazone systems identified using NMR spectroscopy. **b**, **QIH-Me** and **PPH** (1:1) (the signals of the minor *Z* isomer of **PPH** are also labelled). **c**, The mixture of zinc(II)-bound **QIH-Me** and protonated **PPH** obtained after the addition of 1.0 equiv. of $Zn(ClO_4)_2$. **d**–**f**, Protonated **PPH** (**d**), zinc(II)-bound and protonated **QIH-Me** (**e**) and protonated **QIH-Me** (**f**). **g**, Zinc(II)-bound **QIH-Me** and protonated 2,6-di-*tert*-butylpyridine (DBP), **DBP-H$^+$** (the spectrum was recorded after the addition of 1.0 equiv. of $Zn(ClO_4)_2$ to an equimolar mixture of **QIH-Me** and **DBP**).

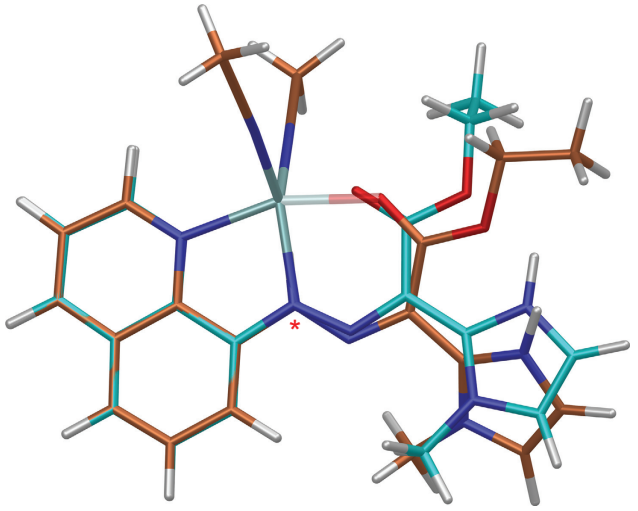

**Figure 6 | Superimposition of the optimized density functional theory (B3LYP/LACV3P**++) structures of QIH-Me(*Z*-H$^+$) (blue) and Zn(QIH-Me(*Z*-H$^+$)) (bronze).** The figure shows the distortion of the molecular framework on coordination to zinc(II), and the tipping of the imidazolium ring out of the plane by 25.5°. The principal site of angular distortion is marked with an asterisk. For simplicity, the calculations were carried out with two acetonitriles coordinated to the metal.

controversial[31,32], that was put forward to explain the lowering of the p$K_a$ of histidine residues in RCs on metal binding (by ~2 units) involves electrostatic repulsion of protons by the bound metal ion. As mentioned earlier, this change in p$K_a$ leads to the slowing down of the photosynthetic cycle in RCs[6–8]. To assess whether conformational changes, electrostatic interactions or other effects are responsible for the behaviour in **Zn(QIH-Me(*Z*-H$^+$))**, we compared closely its X-ray structure with that of **QIH-Me(*Z*-H$^+$)** and that of the previously reported pyridinium system[25], **Zn(QPH(*Z*-H$^+$))**, neither of which are capable of subsequent proton relay (see Supplementary Figs S26 and S27). There seems to be a synergistic effect at play, as both zinc(II) and the imidazolyl ring are required for the reduction in p$K_a$ and switching cascade to take effect. Moreover, we calculated (B3LYP/LACV3P**++) (refs 33–36) the charge distribution in these systems using the natural bond orbital (NBO) method (see Supplementary Information for full details), and used the calculated electron densities at the bond critical points of the intramolecular hydrogen bonds[37] to assess their strengths (see Supplementary Figs S35–S38).

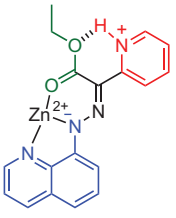

**Zn(QPH(*Z*-H$^+$))**

Comparison of the X-ray and NBO data of the three compounds shows no substantial differences in bond distances or partial charges between them (see Supplementary Table S2), which suggests that inductive and/or resonance effects can be excluded as reasons for the change in p$K_a$. However, the bond critical point calculations show that the hydrogen bond in the non-planar **Zn(QIH-Me(*Z*-H$^+$))** is weaker than that in the zinc(II)-bound and protonated pyridinium system and that in protonated **QIH-Me**. All these data suggest that the change in acidity results from a combination of allosteric and electrostatic effects brought about by the coordination of the switch with zinc(II). The binding event causes the imidazolium ring to tilt out of planarity by 25.5° (Fig. 6), such that the intramolecular hydrogen bond between the imidazolium ring and ester oxygen is weakened relative to that of the other two systems. The lack of a NOESY interaction between the NMe and H2 protons in **Zn(QIH-Me(*Z*-H$^+$))** is an indication that the imidazolium ring also tilts away from planarity when in solution. However, this by itself cannot explain the change in p$K_a$ values and so we hypothesized that the combination of the weakened hydrogen bond with the electrostatic repulsion between the imidazolium proton and zinc(II) results in the observed decrease in the p$K_a$ of the imidazolium ring[8].

To test this hypothesis we synthesized **QPH-Me** (see Supplementary Fig. S6), in which the pyridyl ring is substituted by a methyl group at the 3-position inducing the pyridyl ring to go out of the plane of the molecule (see Supplementary Fig. S39). This substitution drastically changes the isomer ratio in solution (*E*:*Z* = 1:2), which complicates the proton-transfer experiment; the coordination of zinc(II) with the major *Z* isomer will deprotonate the hydrazone NH, which can be picked up directly by **PPH** without switching **QPH-Me**. Nevertheless, **Zn(QPH-Me(*Z*-H$^+$))** can be obtained by adding excess zinc(II) to the latter (see Supplementary Fig. S28). The addition of **PPH** to this solution results in its complete protonation, contrary to no protonation when it is added to the non-methylated version. This experiment shows that the non-planarity (dihedral angle of 132.6(2)° when viewed along the N(4)–C(12)–C(10)=N(2) atoms) of the pyridyl group in **Zn(QPH-Me(*Z*-H$^+$))** (Fig. 3d) is a prerequisite for proton relay to occur. These results indicate that a combination of electrostatic and allosteric effects can be responsible for the change in p$K_a$ observed in RCs on coordination with zinc(II). Moreover, they show that the protons have to be weakly hydrogen bonded for them to be deprotonated on binding of the metal with the RCs, that is, not all titratable protein residues are affected equally by the metal coordination.

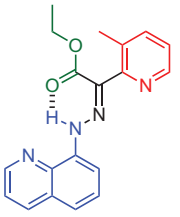

**QPH-Me**

## Conclusions

The field of molecular switches and machines has come a long way in the past two decades[38], but nevertheless quite a few challenges still need to be addressed in the coming years. Of these challenges, using switches to drive systems out of equilibrium[39–41] and integrating them into periodic and robust architectures[42] seem to be the predominant ones. We postulate that the step-wise and congruent activation of different molecular switches is a challenge of equal importance, as this is how complexity[43] is brought about in biological systems. In this article we show that through mimicking biological processes it is possible to effect, using a single input, a multistep switching process (that is, *E*/*Z* isomerizations) that involve two different molecular switches. We show that the switching process is fully reversible, as the addition of cyanide to the hydrazone switch mixture induced a reversal back to its original state.

This reversible multistep switching process opens the way to efficient switching cascades that have minimal side reactions/products as one switch acts as the input to another. The crucial step in the switching process is the lowering of the p$K_a$ of the imidazolyl ring in **QIH-Me** on binding with zinc(II), which results from the

electrostatic repulsion between the metal cation and the weakly hydrogen-bonded proton in the non-planar imidazolium ring. The new insight gained from this system into how to manipulate the $pK_a$ of protonatable residues has far-reaching consequences that will be important for processes that rely on proton relay in their function, such as fuel cells[44] and molecular electrocatalysts[45], among others. Moreover, we can take advantage of the similarities between the effects observed on metal binding in RCs and the imidazolyl-based switch to use the latter as a simple model system for further probing the effect that conformational changes and charge repulsion might have on the relay process in RCs.

Received 15 February 2012; accepted 19 June 2012; published online 29 July 2012

## References


1. Williams, R. J. P. Proton circuits in biological energy interconversions. *Annu. Rev. Biophys. Biophys. Chem.* **17,** 71–97 (1988).
2. Pinto, L. H. *et al.* A functionally defined model for the M2 proton channel of influenza A virus suggests a mechanism for its ion selectivity. *Proc. Natl Acad. Sci. USA* **94,** 6183–6188 (1997).
3. Takeda, M., Pekosz, A., Shuck, K., Pinto, L. H. & Lamb, R. A. Influenza A virus M2 ion channel activity is essential for efficient replication in tissue culture. *J. Virol.* **76,** 1391–1399 (2002).
4. Hu, F., Luo, W. & Hong, M. Mechanisms of proton conduction and gating in influenza M2 proton channels from solid-state NMR. *Science* **330,** 505–508 (2010).
5. Feher, G., Allen, J. P., Okamura, M. Y. & Rees, D. C. Structure and function of bacterial photosynthetic reaction centres. *Nature* **339,** 111–116 (1989).
6. Paddock, M., Graige, M., Feher, G. & Okamura, M. Identification of the proton pathway in bacterial reaction centers: inhibition of proton transfer by binding of $Zn^{2+}$ or $Cd^{2+}$. *Proc. Natl Acad. Sci. USA* **96,** 6183–6188 (1999).
7. Utschig, L., Poluektov, O., Tiede, D. & Thurnauer, M. EPR investigation of $Cu^{2+}$-substituted photosynthetic bacterial reaction centers: evidence for histidine ligation at the surface metal site. *Biochemistry* **39,** 2961–2969 (2000).
8. Gerencsér, L. & Maróti, P. Retardation of proton transfer caused by binding of the transition metal ion to the bacterial reaction center is due to $pK_a$ shifts of key protonatable residues. *Biochemistry* **40,** 1850–1860 (2001).
9. Wei, Y. & Fu, D. Selective metal binding to a membrane-embedded aspartate in the *Escherichia coli* metal transporter YiiP. *J. Biol. Chem.* **280,** 33716–33724 (2005).
10. Wei, Y. & Fu, D. Binding and transport of metal ions at the dimer interface of the *Escherichia coli* metal transporter YiiP. *J. Biol. Chem.* **281,** 23492–23502 (2006).
11. Ohana, E. *et al.* Identification of the $Zn^{2+}$ binding site and mode of operation of a mammalian $Zn^{2+}$ transporter. *J. Biol. Chem.* **284,** 17677–17686 (2009).
12. Dempsey, J. L., Winkler, J. R. & Gray, H. B. Proton-coupled electron flow in protein redox machines. *Chem. Rev.* **110,** 7024–7039 (2010).
13. Kaila, V. R. I., Verkhovsky, M. I. & Wikström, M. Proton-coupled electron transfer in cytochrome oxidase. *Chem. Rev.* **110,** 7062–7081 (2010).
14. Nagle, J. F. & Morowitz, H. Molecular mechanisms for proton transport in membranes. *J. Proc. Natl Acad. Sci. USA* **75,** 298–302 (1978).
15. Le Duc, Y. *et al.* Imidazole-quartet water and proton dipolar channels. *Angew. Chem. Int. Ed.* **50,** 11366–11372 (2011).
16. Chen, Y. *et al.* Enhancement of anhydrous proton transport by supramolecular nanochannels in comb polymers. *Nature Chem.* **2,** 503–508 (2010).
17. Feringa, B. L. *Molecular Switches* (Wiley-VCH, 2001).
18. Kay, E. R., Leigh, D. A. & Zerbetto, F. Synthetic molecular motors and mechanical machines. *Angew. Chem. Int. Ed.* **46,** 72–191 (2007).
19. Balzani, V., Credi, A. & Venturi, M. *Molecular Devices and Machines – Concepts and Perspectives for the Nanoworld* (Wiley-VCH, 2008).
20. Stoddart, J. F. The chemistry of the mechanical bond. *Chem. Soc. Rev.* **38,** 1802–1820 (2009).
21. Breslow, R. Biomimetic chemistry: biology as an inspiration. *J. Biol. Chem.* **284,** 1337–1342 (2009).
22. Landge, S. M. & Aprahamian, I. pH activated configurational rotary switch: controlling the *E*/Z isomerization in hydrazones. *J. Am. Chem. Soc.* **131,** 18269–18271 (2009).
23. Su, X. & Aprahamian, I. Switching around two axles: controlling the configuration and conformation of a hydrazone-based switch. *Org. Lett.* **13,** 30–33 (2011).
24. Landge, S. M. *et al.* Isomerization mechanism in hydrazone-based rotary switches: lateral shift, rotation, or tautomerization? *J. Am. Chem. Soc.* **133,** 9812–9823 (2011).
25. Su, X., Robbins, T. F. & Aprahamian, I. Switching through coordination-coupled proton transfer. *Angew. Chem. Int. Ed.* **50,** 1841–1844 (2011).
26. Schliwa, M. *Molecular Motors* (VCH-Wiley, 2003).
27. Macco, A. A., Godefroi, E. F. & Drouen, J. J. M. 2-(2-imidazolyl)acetophenones. Preparation and some reactions. *J. Org. Chem.* **40,** 252–255 (1975).
28. Pavlović, G., Racané, L., Čičak, H. & Tralić-Kulenović, V. The synthesis and structural study of two benzothiazolyl azo dyes: X-ray crystallographic and computational study of azo–hydrazone tautomerism. *Dyes Pigments* **83,** 354–362 (2009).
29. Gernencer, L., Taly, A., Baciou, L., Maroti, P. & Sebban, P. Effect of binding of $Cd^{2+}$ on bacterial reaction center mutants: proton-transfer uses interdependent pathways. *Biochemistry* **41,** 9132–9138 (2002).
30. Utschig, L. M. & Thurnauer, M. C. Metal ion modulated electron transfer in photosynthetic bacteria. *Acc. Chem. Res.* **37,** 439–447 (2004).
31. Paddock, M. *et al.* Mechanism of proton transfer inhibition by $Cd^{2+}$ binding to bacterial reaction centers: determination of the $pK_a$ of functionally important histidine residues. *Biochemistry* **42,** 9626–9632 (2002).
32. Ishikita, H. & Knapp, E-W. Induced conformational changes upon $Cd^{2+}$ binding at photosynthetic reaction centers. *Proc. Natl Acad. Sci. USA* **102,** 16215–16220 (2005).
33. Jaguar 7.7 (Schrödinger, New York, 2010).
34. Becke, A. D. Density-functional thermochemistry. III. The role of exact exchange. *J. Chem. Phys.* **98,** 5648–5652 (1993).
35. Lee, C., Yang, W. & Parr, R. G. Development of the Colle–Salvetti correlation-energy formula into a functional of the electron density. *Phys. Rev. B* **37,** 785–789 (1988).
36. Hay, P. J. & Wadt, W. R. *Ab initio* effective core potentials for molecular calculations. Potentials for the transition metal atoms Sc to Hg. *J. Chem. Phys.* **82,** 270–283 (1985).
37. Huque, F. T. T. & Platts, J. A. The effects of intramolecular interactions on hydrogen bond acidity. *Org. Biomol. Chem.* **1,** 1419–1423 (2003).
38. Ball, P. Welcome to the machine. *Chem. World* **7,** 56–60 (2010).
39. Astumian, R. D. & Robertson, B. Imposed oscillations of kinetic barriers can cause an enzyme to drive a chemical reaction away from equilibrium. *J. Am. Chem. Soc.* **115,** 11063–11068 (1993).
40. von Delius, M., Geertsema, E. M. & Leigh, D. A. A synthetic small molecule that can walk down a track. *Nature Chem.* **2,** 96–101 (2010).
41. Wang, J. & Feringa, B. L. Dynamic control of chiral space in a catalytic asymmetric reaction using a molecular motor. *Science* **331,** 1429–1432 (2011).
42. Coskun, A., Banaszak, M., Astumian, R. D., Stoddart, J. F. & Grzybowski, B. A. Great expectations: can artificial molecular machines deliver on their promise? *Chem. Soc. Rev.* **41,** 19–30 (2012).
43. Whitesides, G. M. & Ismagilov, R. F. Complexity in chemistry. *Science* **284,** 89–92 (1999).
44. Devanathan, R. Recent developments in proton exchange membranes for fuel cells. *Energy. Environ. Sci.* **1,** 101–119 (2008).
45. Dubois, M. R. & Dubois, D. L. Development of molecular electrocatalysts for $CO_2$ reduction and $H_2$ production/oxidation. *Acc. Chem. Res.* **42,** 1974–1982 (2009).


## Acknowledgements

The authors dedicate this manuscript to Sir Fraser Stoddart on the occasion of his 70th birthday. This work was supported by Dartmouth College, the Burke Research Initiation Award and the American Chemical Society Petroleum Research Fund. The authors thank R. Staples for the X-ray analysis, S. Voskian for his help with the graphic for the table of contents and D.S. Glueck for his input.

## Author contributions

All experiments were conducted by D.R. and J.T.F. with input from I.A. The calculations were carried out and interpreted by R.P.H. The manuscript was co-written by I.A. and D.R. with input from R.P.H.

## Additional information

The authors declare no competing financial interests. Supplementary information and chemical compound information accompany this paper at www.nature.com/naturechemistry. Reprints and permission information is available online at http://www.nature.com/reprints. Correspondence and requests for materials should be addressed to I.A.